International Forum on Aeroelasticity and Structural Dynamics
IFASD 2024
17-21 June 2024, The Hague, The Netherlands

A PROCEDURE FOR FLUTTER ANALYSIS WITH NONLINEAR EXPERIMENTAL MODAL PARAMETERS

Martin Tang[1], Marc Böswald[1]

[1] DLR Institute of Aeroelasticity, Department Structural Dynamics and System Identification, Bunsenstraße 10, 37073 Göttingen

Keywords: GVT, Nonlinear Structural Dynamics, Nonlinear Flutter Analysis

Abstract: GVT are conducted to identify structural modal models which are used afterwards either to validate an existing numerical model or to establish a mathematical substitute model for further analysis, e.g. as input for flutter analysis. The use of experimental substitute models is not based on modelling assumptions. However, the system identification methods applied to the test data are based on the assumptions of linear and time-invariant systems (LTI). Most often nonlinear effects are observed with aerospace structures in a GVT. This would also affect the results of flutter analysis and critical flutter speeds. However, considering nonlinear effects in the analysis model and subsequent nonlinear simulations might not be feasible shortly before the first flight. This work proposes a procedure to perform flutter analysis in time domain with a nonlinear mathematical substitute model, which can be derived from experimental data. A numerical model of a wing section is considered in this work to assess the presented approach. It is shown that LCOs with a fair agreement in amplitude and flight speed of LCO onset in comparison to the nonlinear simulation can be obtained.

1 INTRODUCTION

Aeroelastic stability analysis is an important aspect in aircraft design and certification. For this, numerical models are required which represent the dynamic behavior of the actual structure with sufficient accuracy. A correlation of structural models and experimental results from GVT is conducted before the aeroelastic analysis. If necessary, parameters of the structural model are adjusted in order to improve prediction results [1]. Another approach is to use the experimental modal data, identified from GVT, directly for aeroelastic analysis. However, this method requires accurate modal parameters such as generalized mass and modal damping. But this method would fail when it comes to nonlinear structural dynamics. Aeroelastic stability analysis also assumes linear behavior of the structural model and the aerodynamic model, leading to exponentially growing vibration amplitudes when passing the flutter critical speed. In this respect, nonlinear structural behavior can be beneficial, if for example the system would not show unlimited growth of vibration amplitude, but instead would stabilize at reasonably high amplitudes resulting in limit cycle oscillations (LCO). When the amplitude and the onset speed of the LCO can be predicted, it might be possible to expand the flight envelope [2]. On the contrary, it is also possible that the nonlinear behavior results in reduced flutter speeds for high deflection amplitudes. This is an important feature which must also be known before the first flight.

The nonlinear modelling of mechanical structures is difficult because source and location of nonlinearity is often unknown. Thus, direct usage of nonlinear experimental modal data for aeroelastic analysis is a promising approach, since no assumptions on nonlinear modelling is required. This work investigates whether it is feasible to provide a nonlinear modal model from experimental results and will be illustrated in the following based on a simulation model. The focus will be on the flutter simulation with this substitute model. How those substitutes models are derived experimentally has been indicated in the past [3]. When a nonlinear system is harmonically excited at a given frequency with a given response amplitude, an equivalent linear system can be derived from curve-fitting the nonlinear response with the fundamental harmonic only. This is then repeated for a number of discrete frequencies and amplitudes. From this set of linearized response, a set of linear modal models are derived which are then finally combined to a linear parameter-varying system (LPV) being dependent on the response amplitude itself. Such LPV models can be derived from GVT as well. However, this work does not address the generation of LPV models but instead the use of an LPV model for flutter analysis of a nonlinear system is investigated.

A typical wing section with a nonlinear spring, representing a preloaded gap, at the aileron hinge line is used as proposed by Breitbach [4]. The subsonic unsteady aerodynamics is governed by the Theodorsen function and is transferred to time-domain with the Jones approximation. For this model, a nonlinear simulation is set up and also a simulation with an LPV system approximating the true nonlinear system. Numerical investigations in vacuo with moment excitation as well as aeroelastic time domain analysis are conducted. Both models are then compared to assess whether the LPV system is able to reproduce the results from the nonlinear simulations.

2 THEORETICAL BACKGROUND

Nonlinear assessments are made during GVT in order to characterize the structure under investigation. Those are detected with swept sine excitation or sinusoidal excitation [5]. From those measurements, a nonlinearity curve is derived with eigenfrequency and damping as a function of the strength of excitation. It will be shown how this curve is connected to describing functions and how this is then converted into a simulation model.

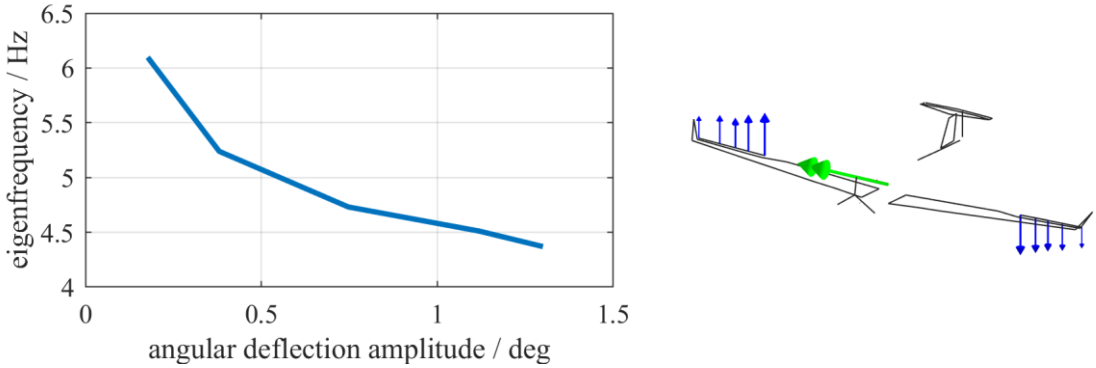

Figure 1 Nonlinearity plot for an aileron mode of a glider from GVT. Left: variation in Eigenfrequency, right: mode shape plot.

Figure 1 left presents the nonlinearity plot for the eigenfrequency of an aileron mode of a glider, measured with normal modes tuning (PRM), as proposed by this author [6]. The force level is stepwise increased and the harmonic excitation frequency is automatically tuned, so the phase lag between excitation force and acceleration response is 90 deg. The angular deflection of the aileron

is estimated from translational acceleration measurements at the hinge line and the trailing edge and the distance between the acceleration sensors. The frequency clearly depends on the actual deflection amplitude and decreases with higher amplitudes. The corresponding mode shape is shown in the right plot in Figure 1. Green arrows in the middle represent the oscillation of the control stick and the blue arrows on the wing illustrate the oscillation of the ailerons. The usage of these experimental findings in further numerical aeroelastic predictions is not straight forward. One could use lowest response level as linearized eigenfrequency for small amplitudes, i.e. underlying linear system. Or assuming highest amplitude response as linear equivalent, since the aircraft must be flutter free for high amplitudes. Best would be the usage of the whole measured curve for subsequent aeroelastic analysis, which requires a nonlinear model reflecting the detected nonlinearity. If a nonlinear model is not available, the direct usage of the measured experimental curve could improve the predictions and simplify the mathematical modelling.

The eigenfrequency shown in Figure 1 depends on the amplitude response of the structure. One theory to describe this behavior are the so-called equivalent harmonic linearization. Within this approach, a harmonic excitation is assumed and the nonlinear response consisting of fundamental and higher harmonics is reduced to the fundamental harmonic response only. This is repeated for varying amplitudes and the relation between all reduced responses and excitations forms the describing function, where one parameter is linearized for each amplitude [7].

An illustrative example of the harmonic linearization is presented in Figure 2. A nonlinear restoring force is shown on the left and on the right the input deflection and output force for 1.5 deg amplitude is displayed, which is in the nonlinear regime of the restoring force. The nonlinear response is projected on the fundamental harmonic and shown as reduced response, which can be interpreted as expansion into a Fourier Series and cut off after the first harmonic. The relation between the input and reduced response is the linearized spring constant for this specific amplitude and harmonic excitation frequency. If this procedure is repeated for a range of different amplitudes, the harmonic linearization or also describing function is derived as shown in Figure 4 for the given amplitudes.

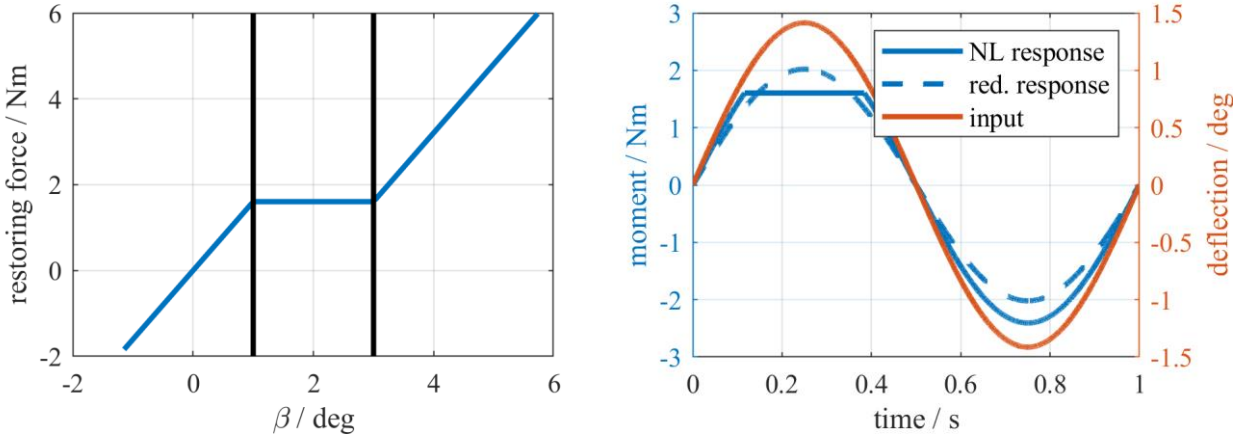

Figure 2 Nonlinear restoring force on the left. Linearization for one given amplitude

Linear parameter-varying systems represent an ensemble of linear models obtained for a grid of discrete values of on one or more governing parameters [8]. As previously discussed, the describing function provides a linearization for a range of different amplitudes. Therefore, the amplitude can be seen as the varying parameter of the system. This establishes a link between the

nonlinearity plot and the describing function. So, the nonlinearity plot, as a result from experiments, can be used to build an LPV model and to run simulations with it. In this case, the parameter depends on the actual deflection of the system itself, whereas originally the governing parameter is an external parameter.

3 SIMULATION MODEL

A typical wing section as shown in Figure 3 and mathematically modelled by Theodorsen [9] is used for the illustration of the presented approach. It consists of three degrees of freedom with plunge, pitch and aileron rotation. Subsonic flow is assumed so that potential theory is applicable. The indicated position of the elastic axis a and hinge axis c are normalized with the semi chord length b. The dynamics are driven by the structural dynamics as described in Eq. (1) and the unsteady aerodynamics as shown in Eq. (2). The matrix notation is inspired by Perry [10]. The Theodorsen function lags the circulatory forces and is formulated in the frequency domain and are approximated according to Jones, as given by Brunton [11] in state space form. Breitbach [4] added nonlinear springs in order to study the nonlinear dynamics of the wing section. The example with preloaded free play as depicted in Figure 2 is used within this work.

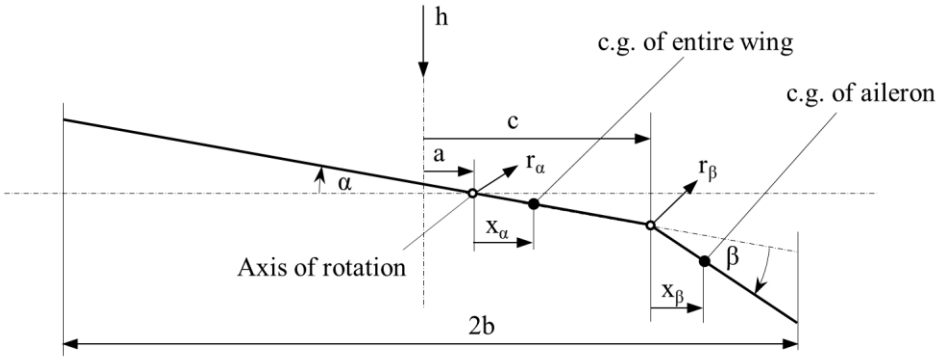

Figure 3 Wing section described by Theodorsen [9]

The equations given by Theodorsen read

$$A_s\ddot{q} + B_s\dot{q} + C_s q = P \tag{1}$$

$$A_{nc}\ddot{q} + B_{nc}\dot{q} + C_{nc}q + C(k)[A_c\ddot{q} + B_c\dot{q} + C_c q] = P, \tag{2}$$

where q is the deflection vector of the wing section and A, B, C are coefficient matrices. Subscript s denotes the structural matrices. The subscript nc denotes the noncirculatory matrices for the unsteady aerodynamics, which act directly on the structure. Finally, subscript c denotes the circulatory part of the aerodynamic forces, which is lagged by the Theodorsen function C(k). The deflection vector is defined as (see Figure 3 for orientation):

$$q = [h \quad \alpha \quad \beta]^T \tag{3}$$

And the structural coefficient matrices are

$$A_s = \begin{bmatrix} M & S_\alpha & S_\beta \\ S_\alpha & I_\alpha & I_\beta + b(c-a)S_\beta \\ S_\beta & I_\beta + b(c-a)S_\beta & I_\beta \end{bmatrix}$$
$$B_s = \begin{bmatrix} c_h & 0 & 0 \\ 0 & c_\alpha & 0 \\ 0 & 0 & c_\beta \end{bmatrix} \text{ and } C_s = \begin{bmatrix} k_h & 0 & 0 \\ 0 & k_\alpha & 0 \\ 0 & 0 & k_\beta \end{bmatrix} \quad (4)$$

where k denotes the stiffness for each degree of freedom and c the damping coefficients, which are usually set to zero. The inertia properties in A_s are given in Theodorsen [9].

The aerodynamic coefficient matrices for the noncirculatory part are

$$A_{NC} = -\rho b^2 \begin{bmatrix} \pi & -\pi b a & 2\,T_{10} \\ -2\pi b\left(a+\frac{1}{2}\right) & \pi b^2\left(\frac{1}{8}+a^2\right) & -(T_7+(c-a)T_1)b^2 \\ -T_1\,b & 2\,T_{13}\,b^2 & -\frac{1}{pi}T_3\,b^2 \end{bmatrix}$$

$$B_{NC} = -\rho b^2 v \begin{bmatrix} 0 & \pi & -T_4 \\ 0 & \pi\left(\frac{1}{2}-a\right)b & \left(T_1 - T_8 - (c-a)T_4 + \frac{1}{2}T_{11}\right)b \\ 0 & \left(-2\,T_9 - T_1 + T_4\left(a-\frac{1}{2}\right)\right)b & -\frac{1}{2\pi}b\,T_4\,T_{11} \end{bmatrix} \quad (5)$$

$$C_{NC} = -\rho b^2 v^2 \begin{bmatrix} 0 & 0 & 0 \\ 0 & 0 & T_4 + T_{10} \\ 0 & 0 & \frac{1}{\pi}(T_5 - T_4\ T_{10}) \end{bmatrix}$$

The coefficient matrices of the circulatory term are

$$A_C = [0]$$

$$B_C = -\rho b v \begin{bmatrix} 2\pi & 2\pi b\left(\frac{1}{2}-a\right) & b\,T_{11} \\ -2\pi b\left(a+\frac{1}{2}\right) & -2\pi b^2\left(a+\frac{1}{2}\right)\left(\frac{1}{2}-a\right) & -b^2\left(a+\frac{1}{2}\right)T_{11} \\ b\,T_{12} & b^2\,T_{12}\left(\frac{1}{2}-a\right) & \frac{b^2}{2\pi}T_{11}\,T_{12} \end{bmatrix} \quad (6)$$

$$C_C = -\rho b v^2 \begin{bmatrix} 0 & 2\pi & 2\,T_{10} \\ 0 & -2\pi b^2\left(a+\frac{1}{2}\right) & -2b\,T_{10}\left(a+\frac{1}{2}\right) \\ 0 & b\,T_{12} & \frac{b}{\pi}T_{12}\,T_{10} \end{bmatrix}$$

The T coefficient are given by Theodorsen [9].

Figure 2 plots the nonlinear restoring force of the spring at the aileron, as proposed by Breitbach [4]. It is a preloaded free play, where the gap ranges from 1 deg to 3 deg. Figure 4 presents the describing function of the nonlinear spring with respect to harmonic motion with zero mean value and variable deflection amplitude. The decrease in stiffness indicates a decrease in eigenfrequency as observed in the measured eigenfrequency over amplitude plot in Figure 1.

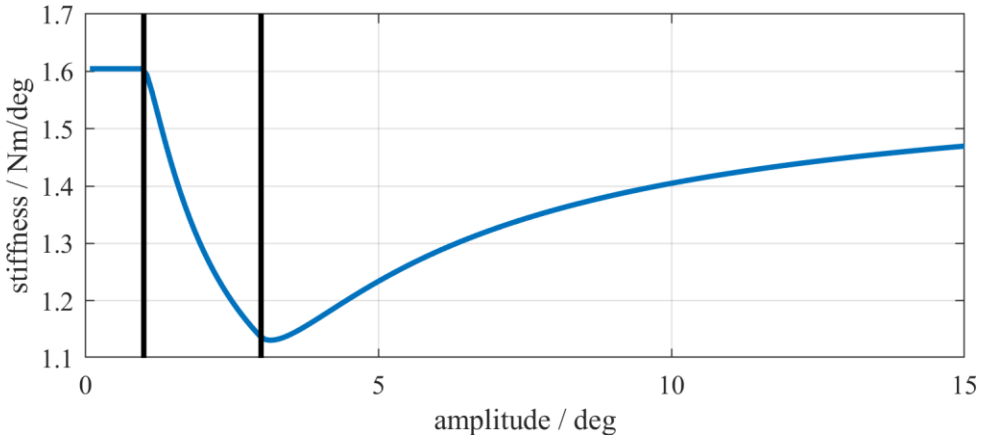

Figure 4 describing function of nonlinear spring

A drop of the equivalent stiffness is seen when the deflection amplitude reaches the entry of the gap at 1 deg. If the deflection amplitude exceeds 3 deg, the stiffness increases again since the restoring force also increases again as the end of the gap is passed.

For the numerical investigations two simulation models of the structure have been set up in Simulink. One model represents the full nonlinear system with the nonlinear restoring force, whereas the other simulation model is represented as a modal LPV system and depends on the deflection amplitude of the system itself. Both models of the structure are then coupled with the same linear unsteady aerodynamics based on the equations of Theodorsen and the Jones approximation.

The equations for the structural dynamics are recasted into state space form as follows:

$$\begin{aligned} \dot{x}_e &= A_e^{ss} x_e + B_e^{ss} u_e \\ y_e &= C_e^{ss} x_e + D_e^{ss} u_e, \end{aligned} \tag{7}$$

with x_e being the state vector consisting of deflection and velocity for the three degrees of freedom. And y_e comprises acceleration, velocity and displacement as output quantities. The input u_e represents the forces and moments acting on the wing section. One force and moment act on the elastic axis and one moment act on the hinge axis of the aileron. The system matrices are

$$\begin{aligned} A_e^{SS} &= \begin{bmatrix} O & I \\ -A_s^{-1}C_s & -A_s^{-1}B_s \end{bmatrix}, B_e^{SS} = \begin{bmatrix} O \\ A_s^{-1} \end{bmatrix} \\ C_e^{SS} &= \begin{bmatrix} -A_s^{-1}C_s & -A_s^{-1}B_s \\ O & I \\ I & O \end{bmatrix}, D_e^{SS} = \begin{bmatrix} A_s^{-1} \\ O \\ O \end{bmatrix} \end{aligned} \tag{8}$$

The unsteady aerodynamics are also put into the form of a state space model with the structural deflection, velocity and acceleration as input u_a and the three forces and moments as ouput y_a, so that structural dynamics and unsteady aerodynamics can be put into a feedback loop, as shown in Figure 5.

$$\begin{aligned} \dot{x}_a &= A_a^{ss} x_a + B_a^{ss} u_a \\ y_a &= C_a^{ss} x_a + D_a^{ss} u_a, \end{aligned} \tag{9}$$

The matrices B, C and D are derived from Eq. (2) and matrix A is given by the Jones approximation from Brunton [11]. The state space representation of the Jones approximation reads

$$\begin{aligned} A_0^{SS} &= \frac{v}{b}\begin{bmatrix} -0.3455 & -0.01365 \\ 1 & 0 \end{bmatrix}, B_0^{SS} = \begin{bmatrix} 1 \\ 0 \end{bmatrix} \\ C_0^{SS} &= \frac{v}{b}[0.1081 \quad 0.006852] \text{ and } D_0^{SS} = 0.5 \end{aligned} \tag{10}$$

Matrix A and C are scaled by v/b in order to transform the Jones approximation to dimensioned angular frequencies according to $\omega = k\frac{v}{b}$.

Finally, the system matrices for the unsteady aerodynamics results in

$$\begin{aligned} A_a^{SS} &= I \otimes A_0^{SS}, B_a^{SS} = [A_{NC} \quad B_{NC} \quad C_{NC}] \otimes B_0^{SS} \\ C_a^{SS} &= I \otimes C_0^{SS}, D_a^{SS} = D_0^{SS}[A_{NC} \quad B_{NC} \quad C_{NC}] \end{aligned} \tag{11}$$

with $\otimes$ being the Kronecker product. The Kronecker product expands the state space model given by eq. (10) so that the three circulatory forces are lagged separately.

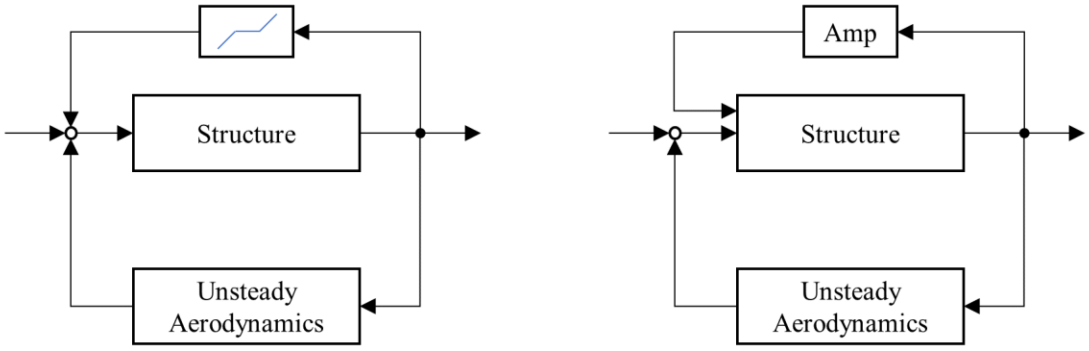

Figure 5 Block diagrams for simulation models. Left: nonlinear model; right: LPV model with amplitude estimate

Figure 5 presents the architecture of the simulation models used in Simulink. The left side shows the nonlinear model, where the actual deflection of the aileron is fed back through the nonlinear function depicted in Figure 2 left. The aileron stiffness in the system matrix is set to zero in this case. The right graph shows the architecture of the LPV model, where the system matrices are dependent on the actual amplitude of the aileron deflection, as depicted in Figure 4. The amplitude of the aileron deflection is estimated as scaled root mean square ($\sqrt{2}\,RMS$) of the aileron response, as shown in Eq. (12).

This equation is implemented as discrete filter, which allows an online estimate of the aileron deflection in order to adjust the LPV system in accordance to the current response amplitude. However, the length of the time window T has to be chosen as an additional parameter and is an integer multiple of the discrete time step.

$$A_\beta = \sqrt{\frac{2}{T}\int_{t-T}^{t} \beta(t)^2 \, dt}, \tag{12}$$

4 RESULTS

This section describes the results from the simulation model. A comparison between the LPV model against the full nonlinear model is conducted, in order to assess whether the linearization is able to capture the nonlinear effects. First, the unsteady aerodynamics is not considered and in vacuo force excitation is tested with different sweep excitation levels. From GVT, only a mechanical substitute model is identified, so this mathematical model is verified from those simulations. Then, aeroelastic simulations are conducted, to assess the ability of the LPV model to also predict LCO responses.

4.1 Mechanical Simulations

4.1.1 Linearized Analysis

The linear system with small amplitude response is described first. Looking at Figure 4, one can see that the spring behaves linearly if the aileron deflection response remains below 1 deg. For the linear system, the first eigenfrequency at 3.56 Hz is the plunge mode, as presented in Figure 6 left. The second mode results in pitch with aileron deflection at 15.3 Hz as shown in the middle. At 18.1 Hz the aileron deflection is seen as depicted on the right. In contrast to the example shown in Figure 1, the aileron mode is located at rather high frequency, even above the pitch mode. The high eigenfrequency can be explained with a different mounting of the aileron with the wing in comparison to the glider shown in the beginning.

Table 1 modal parameters of the wing section

	Heave	**Pitch**	**Aileron**
eigenfrequency	3.56 Hz	15.3 Hz	18.1 Hz

Figure 6 Mode shapes of the wing section

As response amplitudes of the aileron exceed 1 deg, the entry of the gap is reached and the spring softens, as indicated in Figure 4. Linearizing the system at different amplitude levels and recomputing the modal properties results in a drop of frequencies with amplitudes around the gap and increase of eigenfrequencies above 3 deg aileron deflection again, as shown in Figure 7 on the

left. The wing bending around 3.5 Hz is not affected at all, whereas the aileron mode at 18 Hz clearly changes in frequency. However, the wing torsion around 15 Hz is also affected by the aileron stiffness, since the aileron is also participating in the mode shape as seen in Figure 6 in the middle. The mode shapes also remain very similar in appearance as sown in Figure 7 right, where the MAC value is shown over the aileron deflection amplitude with respect to the linear case. The pitch mode drops around 2% in MAC if the aileron oscillates within the gap, means that the mode shape is not changing a lot with deflection amplitude.

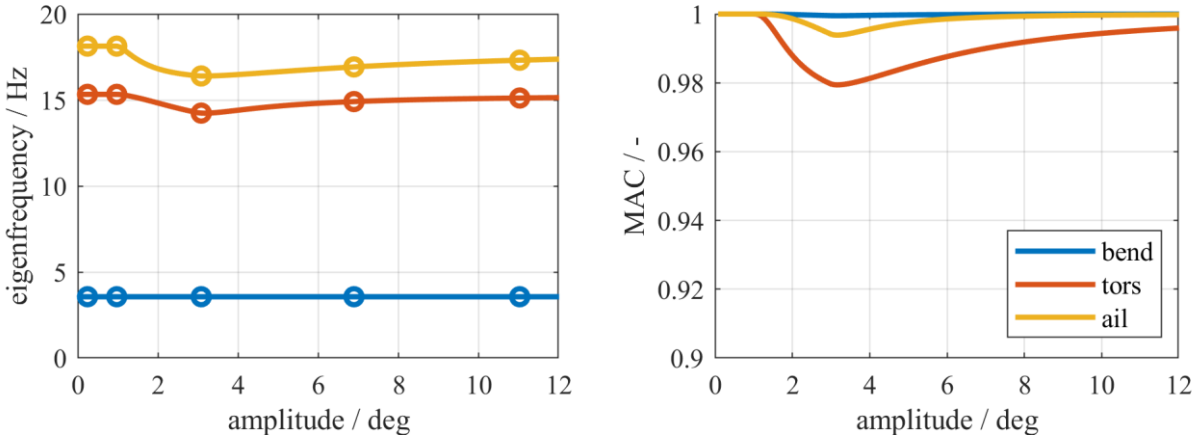

Figure 7 left:eigenfrequencies with respect to aileron deflection ampiltude. Right: MAC values referenced to linear modes.

With eigenfrequencies, mode shapes and modal masses, it is possible to build modal models for each response amplitude of the aileron. Figure 7 left indicates the 5 mode sets chosen for the LPV model of the structure representing the nonlinear system. Those amplitudes at which the mode sets are chosen capture significant points, such as the beginning of the drop in eigenfrequency when the aileron enters the gap and the amplitude with the minimal equivalent stiffness. The LPV model interpolates linearly in between. For the simulations of the mechanical system only, 2 % modal damping has been applied to the linear system in order to enable damped response of the system.

4.1.2 Nonlinear Response Simulations

The simulation models shown in Figure 5 without unsteady aerodynamics are utilized to compute responses to swept sine moment excitation at the aileron. Three excitation levels are chosen to assess the applicability of the LPV model. For the first excitation level linear response is expected. At the second excitation level a softening effect is expected, where aileron runs into the gap, and the third excitation level a stiffening effect is expected, when the aileron leaves the gap again.

The time step has been set to 10^{-4} s for the nonlinear simulation. In a sensitivity study it has been verified, that the results remain similar if time step is further reduced. The sweep rate is set to 0.5 Oct/min and the first level is 0.01 Nm to ensure linear behavior. As input location, the aileron has been chosen. Now, the simulation model is replaced by the LPV model. The estimate of the amplitude of the aileron deflection for the state of the LPV model is crucial. If the filter length is too long, the delay is too high and the dynamics are not appropriately represented. If it is too short, the amplitude is not estimated correctly or tends to oscillate. As a compromise, the averaging time T from Eq. (12) is chosen to be 0.02 s.

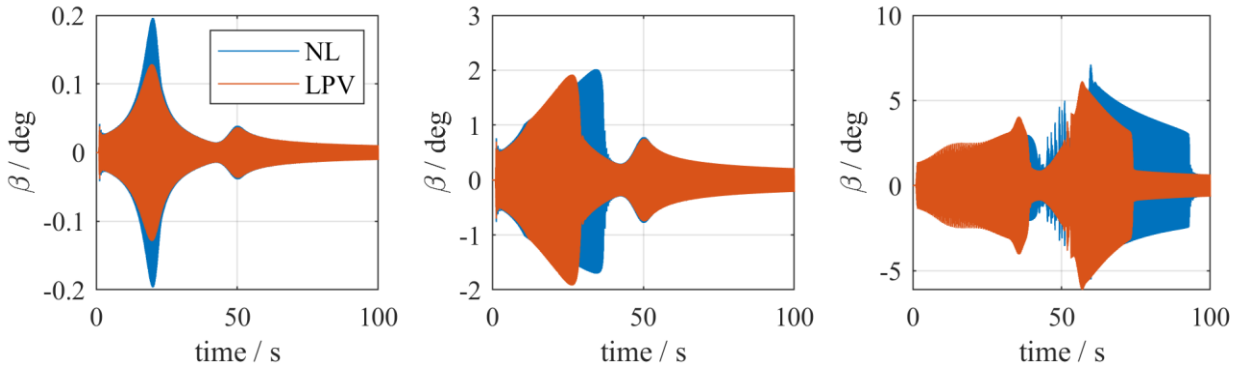

Figure 8 time domain simulations. Increasing excitation level from left to right (0.01Nm, 0.2Nm and 0.6Nm).

Figure 8 shows the results from simulations at the three excitation levels. The signal shown is the deflection of the aileron. The down sweep excites the aileron mode first and then the pitch mode. The result on the left shows linear response. It seems that the LPV system has more damping. The plot in the middle with 0.2 Nm excitation force shows that the LPV system is able to capture also nonlinear behavior. However, the jump is predicted at a different point in time, which might be related to the amplitude estimate of the LPV simulation. But the amplitude at which the jumps occurs is approximately the same. The right plot shows the results for the highest force level at 0.6Nm, where both modes are exhibiting nonlinear behavior, as indicated in Figure 7. Again, the LPV system is able to represent the same dynamic behavior, although damping seems to be slightly higher and also the jump of the response is predicted at a different point in time but approximately at the same response amplitude, probably due to the different damping seen in the linear response. Additionally, the responses in the nonlinear simulations show higher harmonics in the nonlinear regime, whereas the LPV system is a combination of linear systems and thus, the response does not include higher harmonics due to the nonlinear spring.

4.2 Aeroelastic Simulations

4.2.1 Linearized Flutter Analysis

It has been seen in the previous section, that the LPV system is able to represent the nonlinear system to some extent. This section includes the aerodynamics as proposed by Theodorsen with linearization through Jones approximation. The stability analysis of the linear system is presented first.

Figure 9 shows the results for the flutter analysis of the wing section with small response amplitudes. The blue line represents the aileron mode which turns unstable at around 85 m/s. The yellow line represents the pitch mode and the green line represents the bending mode. For both modes, the damping increases with increasing free stream velocity.

Figure 10 shows the results for a reduced stiffness at the aileron hinge line with a deflection amplitude around 3 deg, as indicated in Figure 4. One can see that the initial eigenfrequencies are lower and also the evolution with free stream velocity is slightly different. No crossing between the frequencies of aileron and pitch mode appears anymore. More importantly, the aileron mode becomes unstable around 80 m/s. The system stiffens again with higher amplitude, which means that a limit cycle oscillation is expected here, because flutter speed should also increase again with increasing stiffness.

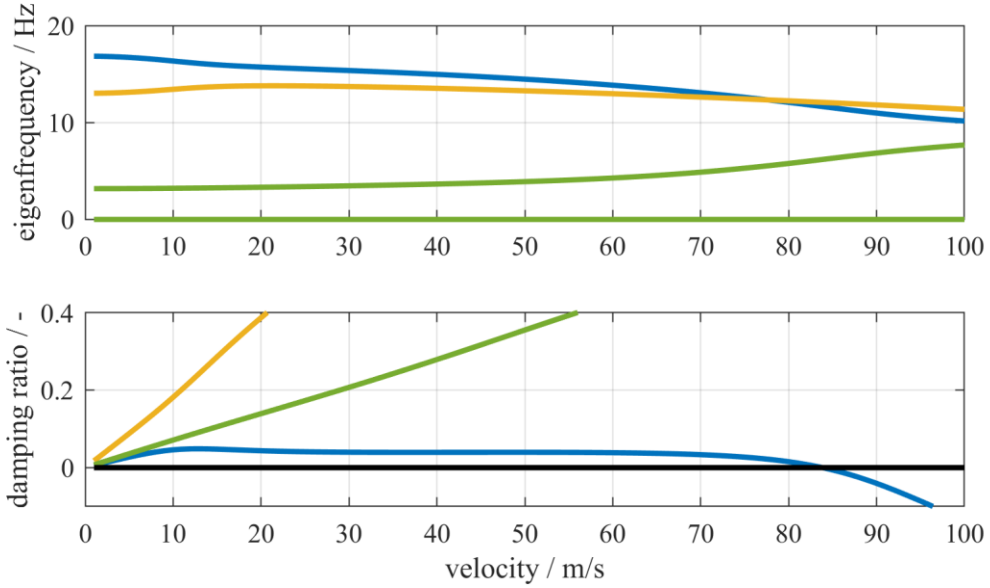

Figure 9 stability diagram for the wing section

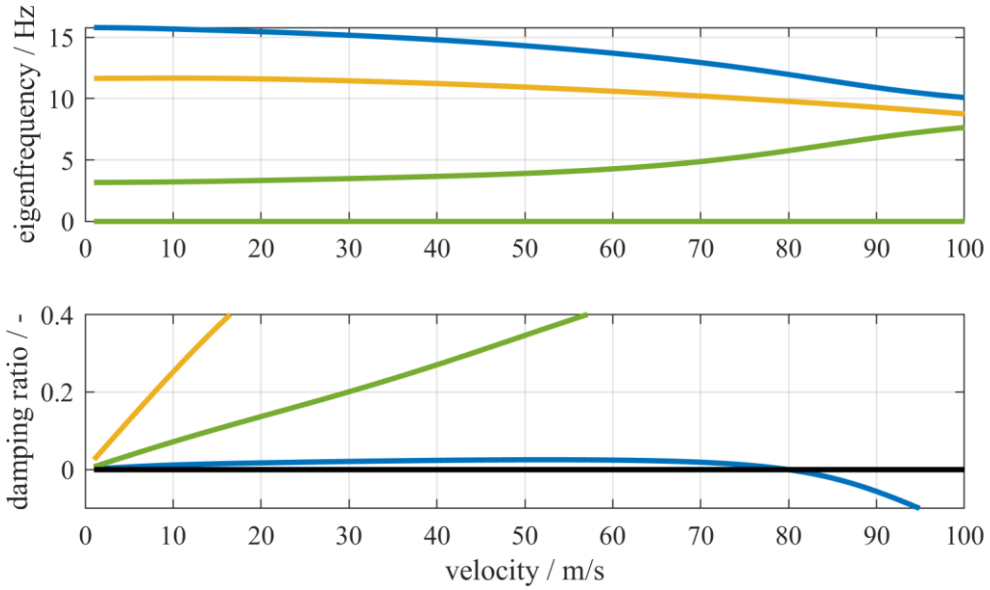

Figure 10 stability diagram for the wing section with reduced aileron stiffness

This is illustrated in Figure 11. The zero crossing in the damping in Figure 10 are found for different stiffness variations at different response amplitudes from Figure 7. The dark region represents the unstable regime and the bright region is stable. It is seen, that the wing section becomes unstable at lower free stream velocity when aileron amplitudes increase. The minimum flutter speed is reached at 3 deg aileron deflection amplitude around 80 m/s. After passing the 3 deg deflection amplitude, the flutter speed increases again. Up to 83 m/s LCOs can occur. For example, if the wing section becomes unstable at 82 m/s, the aileron deflection increases and stabilizes itself again at a certain amplitude, so that an LCO occurs. It shall be noted that the shape

of the boundary between the stable and the unstable regimes in Figure 11 looks similar to the shape of the describing function of the nonlinear spring shown in Figure 4.

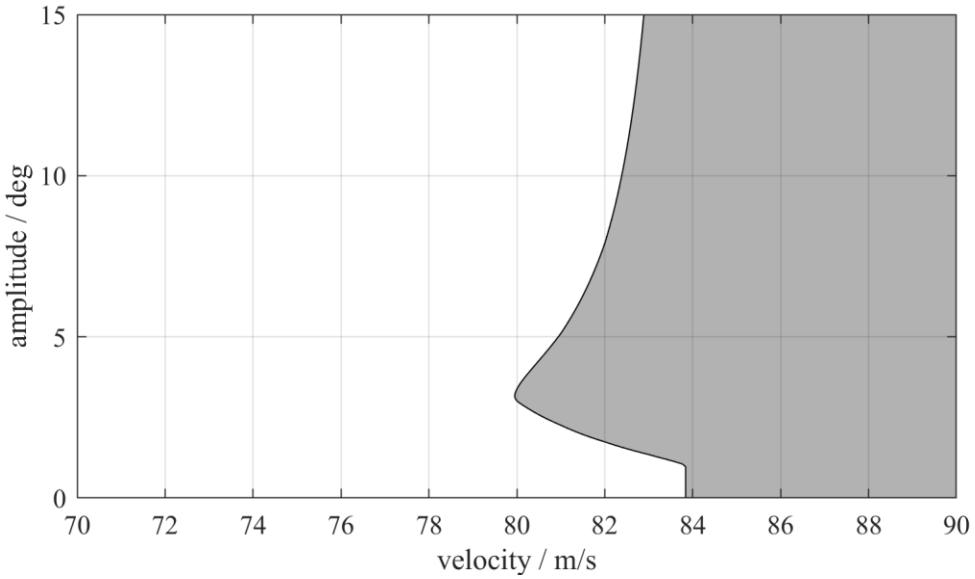

Figure 11 stability chart with respect to aileron deflection and velocity

4.2.2 Nonlinear Time Domain Simulations at 82 m/s

For the LPV system, the coupling has been conducted for each linearization, resulting in 5 coupled aeroelastic models. Again, the amplitude of the aileron deflection is fed back for the LPV system. For the nonlinear simulation, the time step has been reduced to 10^{-5} s, since the simulation time was shorter. The time step for the LPV model stays at 10^{-4} s. As disturbance, a 1-cos moment pulse at the aileron with different excitation level is chosen. The frequency of the 1-cos pulse was chosen to be 15 Hz.

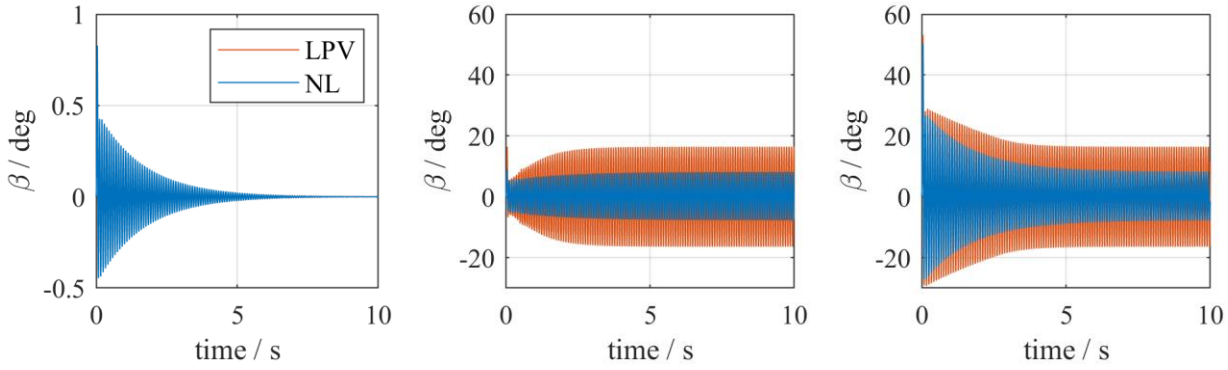

Figure 12 time domain simulations of the aeroelastic system at 82 m/s. Increasing disturbance from left to right (4Nm, 40Nm and 240Nm)

Figure 12 shows the aileron deflection after applying the disturbance for the two systems. For a small disturbance of 4 Nm, both simulations show the same decay. If the disturbance is increased to 40 Nm, an LCO occurs and is predicted from both systems. However, the response of the LPV

system is estimated at a higher amplitude. The nonlinear system response is around 7 deg in accordance with Figure 11. The LPV system on the other hand gives an amplitude of 16 deg. Increasing the disturbance even more to 240 Nm amplitude, the result on the right is obtained. The response is decaying until the LCO amplitude is reached. Again, a difference in amplitude for both systems agree to the middle plot. The overall behavior is predicted well by the LPV system. The decay observed is in correspondence with Figure 11, as the starting point is in a stable region and the deflection decreases until it reaches a damping of zero.

The eigenfrequency of the LCO for the LPV system is at 11.84 Hz and from the nonlinear analysis at 11.76 Hz. The amplitude distribution of the three degree of freedom are for both simulations very similar and the same applies for their phase lag amongst each other. The Results for the LCO mode are summarized in Table 2. So, the LCO mode is predicted well by the LPV system.

Table 2 LCO amplitude ratios and phase lag to aileron response.

	Heave	**Pitch**	**Aileron**
NL (11.84 Hz)	*0.20 (170 deg)*	0.86 (107 deg)	1 (0 deg)
LCO (11.76 Hz)	*0.21 (173 deg)*	0.88 (109 deg)	1 (0 deg)

Figure 13 shows the result for the nonlinear simulation at 83 m/s and the LPV simulation at 82 m/s. The disturbance set to 40 Nm and the LCO amplitude is now in good agreement as well. From Figure 11, the sensitivity of the LCO can be seen. The LCO amplitude is given by the upper line and increases a lot with increasing wind speed, meaning that this parameter is very sensitive to wind speed changes.

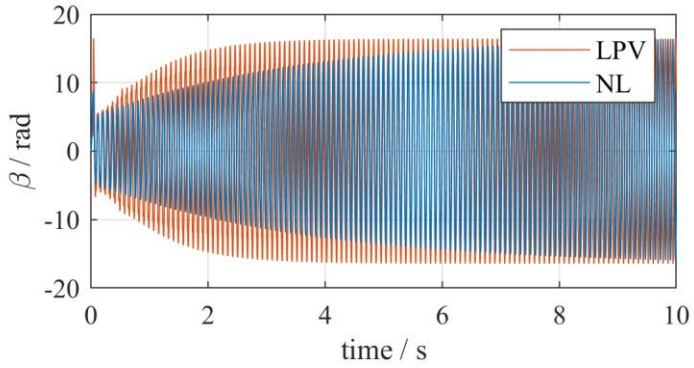

Figure 13 comparison of LPV at 82 m/s and nonlinear simulation at 83 m/s

5 CONCLUSIONS

In linear aeroelasticity the flutter analysis can be conducted with modal models identified from test data. This does not work anymore for nonlinear structures. However, this work gives a proof of concept for a procedure that does not rely on a nonlinear structural model. Instead, the nonlinear effects are covered by an ensemble of linear substitute models arranged in an LPV system. Such an LPV system can be established from experimental modal analysis as it has been indicated in the past [3].

A wing section with three degrees of freedom, as it is presented by Theodorsen, is used for demonstration purposes. The aileron stiffness has been replaced with a nonlinear spring

representing a preloaded gap. This example has been proposed by Breitbach and the simulation results could be reproduced (Figure 11). From describing function analysis, equivalent linear modal models for different amplitude levels of the aileron deflection are derived and assembled into an LPV system. The blending from one equivalent linear model to another one is controlled in this case by the actual deflection amplitude of the aileron. This LPV system can be also assembled from experimental modal data measured at different constant response amplitude levels. Purely mechanical simulations and aeroelastic simulations have been conducted and it was shown that the qualitative behavior of the nonlinear system can be captured by this simplified LPV model, although the amplitude predictions are different.

In this case, the LPV system has been generated from five equivalent linear systems. During the simulation, the response analysis has to switch from the one linear system to another one. When using LPV in Simulink, this is all controlled automatically. But in fact, the quality of the numerical simulation with LPV systems largely depends on the number of equivalent linear systems and on the location of the discrete points in the amplitude range. In this example, the describing function was known a priori and the distinct amplitudes to blend from the one equivalent linear system to another one was chosen accordingly. However, in a real experiment the describing function is not known a priori and thus the required number of equivalent linear systems and the discrete points in the range of amplitudes might be difficult to find. Nonetheless, effort has to be spent to obtain an experimental describing function of a nonlinear mode of a structure. Once this is available, the number of discretization points and their distribution in the amplitude range can be optimized based on the curvature of the describing function.

REFERENCES

[1] Mottershead, J. E., Link, M., Friswell, M. I., and Schedlinski, C., "Model Updating," *Handbook of Experimental Structural Dynamics*, edited by R. Allemang and P. Avitabile, Springer New York; Imprint Springer, New York, NY, 2020, pp. 1–53.

[2] EASA, "Proposed Special Condition for Installation of Flutter Suppression System - Applicable to Boeing 747-8 / -8F," 11.05.2011, SC C-18, https://www.easa.europa.eu/sites/default/files/dfu/SC%20C-18%20for%20publication.pdf.

[3] Tang, M., Böswald, M., and Govers, Y., "Phase resonance method for linearized identification of nonlinear mechanical structures," *19th International Forum on Aeroelasticity and Structural Dynamics, IFASD 2022*, 2022.

[4] Breitbach, E. J., "Flutter analysis of an airplane with multiple structural nonlinearities in the control system," NASA-TP-1620, 3 Jan. 1980, https://ntrs.nasa.gov/citations/19800015832.

[5] Gloth, G., and Sinapius, M., "Influence and characterisation of weak non-linearities in swept-sine modal testing," *Aerospace Science and Technology* [online], Vol. 8, No. 2, 2004, pp. 111–120, https://www.sciencedirect.com/science/article/pii/S1270963803000956.

[6] Tang, M., Stéphan, C., and Böswald, M., "Phase resonance method for nonlinear mechanical structures with phase locked loop control," *Proceedings of the ISMA 2020, International Conference on Noise and Vibration Engineering/USD 2020, International Conference on Uncertainty in Structural Dynamics*, KU Leuven Department of Mechanical Engineering, Heverlee (Belgium), 2020, pp. 1805–1818.

[7] vander Velde, W. E., and Gelb, A., *Multiple-input describing functions and nonlinear system design*, 1968.

[8] Shamma, J. S., “An Overview of LPV Systems,” *Control of Linear Parameter Varying Systems with Applications,* edited by J. Mohammadpour and C. W. Scherer, Springer US, Boston, MA, 2012, pp. 3–26.
[9] Theodorsen, T., “General Theory of Aerodynamic Instability and the Mechanism of Flutter,” NACA-TR-496, 1 Jan. 1949, https://ntrs.nasa.gov/citations/19930090935.
[10] Perry, Boyd, III, “Comparison of Theodorsen's Unsteady Aerodynamic Forces with Doublet Lattice Generalized Aerodynamic Forces,” NASA/TM-2017-219667, 9 Jan. 2017, https://ntrs.nasa.gov/citations/20170009599.
[11] Brunton, S. L., and Rowley, C. W., “Empirical state-space representations for Theodorsen's lift model,” *Journal of Fluids and Structures* [online], Vol. 38, 2013, pp. 174–186, https://www.sciencedirect.com/science/article/pii/S0889974612002010.

COPYRIGHT STATEMENT